AFRL-RX-WP-TP-2011-4416

AGILE THERMAL MANAGEMENT STT-RX Themophysical Properties of Lithium Nitrate Trihydrate from - 20 degrees C to 80 degrees C (PREPRINT)

Patrick J. Shamberger
Nonmetallic Materials Division
Thermal Sciences & Materials Branch

Timothy Reid
University of Dayton Research Institute

DECEMBER 2011

Approved for public release; distribution unlimited.
See additional restrictions described on inside pages

STINFO COPY

AIR FORCE RESEARCH LABORATORY
MATERIALS AND MANUFACTURING DIRECTORATE
WRIGHT-PATTERSON AIR FORCE BASE, OH 45433-7750
AIR FORCE MATERIEL COMMAND
UNITED STATES AIR FORCE

NOTICE AND SIGNATURE PAGE

Using Government drawings, specifications, or other data included in this document for any purpose other than Government procurement does not in any way obligate the U.S. Government. The fact that the Government formulated or supplied the drawings, specifications, or other data does not license the holder or any other person or corporation; or convey any rights or permission to manufacture, use, or sell any patented invention that may relate to them.

This report was cleared for public release by the USAF 88th Air Base Wing (88 ABW) Public Affairs Office and is available to the general public, including foreign nationals. Copies may be obtained from the Defense Technical Information Center (DTIC) (http://www.dtic.mil).

AFRL-RX-WP-TR-2011-4416 HAS BEEN REVIEWED AND IS APPROVED FOR PUBLICATION IN ACCORDANCE WITH ASSIGNED DISTRIBUTION STATEMENT.

//SIGNED//

KARLA STRONG, Program Manager
Thermal Sciences and Materials Branch
Nonmetallic Materials Division

//SIGNED//

NADER HENDIZADEH, Chief
Thermal Sciences and Materials Branch
Nonmetallic Materials Division

//SIGNED//

SHASHI K. SHARMA, Deputy Chief
Nonmetallic Materials Division
Materials and Manufacturing Directorate

This report is published in the interest of scientific and technical information exchange, and its publication does not constitute the Government's approval or disapproval of its ideas or findings.

*Disseminated copies will show "//signature//" stamped or typed above the signature blocks.

REPORT DOCUMENTATION PAGE

Form Approved
OMB No. 0704-0188

The public reporting burden for this collection of information is estimated to average 1 hour per response, including the time for reviewing instructions, searching existing data sources, searching existing data sources, gathering and maintaining the data needed, and completing and reviewing the collection of information. Send comments regarding this burden estimate or any other aspect of this collection of information, including suggestions for reducing this burden, to Department of Defense, Washington Headquarters Services, Directorate for Information Operations and Reports (0704-0188), 1215 Jefferson Davis Highway, Suite 1204, Arlington, VA 22202-4302. Respondents should be aware that notwithstanding any other provision of law, no person shall be subject to any penalty for failing to comply with a collection of information if it does not display a currently valid OMB control number. **PLEASE DO NOT RETURN YOUR FORM TO THE ABOVE ADDRESS**.

1. REPORT DATE *(DD-MM-YY)*	2. REPORT TYPE	3. DATES COVERED *(From - To)*
December 2011	Technical Paper	1 November 2011 – 1 November 2011

4. TITLE AND SUBTITLE
AGILE THERMAL MANAGEMENT STT-RX
Themophysical Properties of Lithium Nitrate Trihydrate from - 20 degrees C to 80 degrees C (PREPRINT)

5a. CONTRACT NUMBER
In-house

5b. GRANT NUMBER

5c. PROGRAM ELEMENT NUMBER
62102F

6. AUTHOR(S)
Patrick J. Shamberger (AFRL/RXBT)
Timothy Reid (University of Dayton Research Institute)

5d. PROJECT NUMBER
4347

5e. TASK NUMBER
62

5f. WORK UNIT NUMBER
BT110100

7. PERFORMING ORGANIZATION NAME(S) AND ADDRESS(ES)
Nonmetallic Materials Division
Thermal Sciences& Materials Branch
Air Force Research Laboratory, Materials and Manufacturing Directorate
Wright-Patterson Air Force Base, OH 45433-7750
Air Force Materiel Command, United States Air Force

University of Dayton Research Institute

8. PERFORMING ORGANIZATION REPORT NUMBER
AFRL-RX-WP-TP-2011-4416

9. SPONSORING/MONITORING AGENCY NAME(S) AND ADDRESS(ES)
Air Force Research Laboratory
Materials and Manufacturing Directorate
Wright-Patterson Air Force Base, OH 45433-7750
Air Force Materiel Command
United States Air Force

10. SPONSORING/MONITORING AGENCY ACRONYM(S)
AFRL/RXBT

11. SPONSORING/MONITORING AGENCY REPORT NUMBER(S)
AFRL-RX-WP-TP-2011-4416

12. DISTRIBUTION/AVAILABILITY STATEMENT
Approved for public release; distribution unlimited.

13. SUPPLEMENTARY NOTES
The U.S. Government is joint author of this work and has the right to use, modify, reproduce, release, perform, display, or disclose the work. PA Case Number and clearance date: 88ABW-2011-5821, 02 Nov 2011. Preprint journal article to be submitted to Journal of Chemical Engineering Data. This document contains color.

14. ABSTRACT
Lithium nitrate trihydrate is of interest as a thermal energy storage material, due to its large specific and volumetric heats of fusion and its low melting temperature. Here, we report the thermophysical properties of solid and liquid lithium nitrate trihydrate at temperatures between -20 °C and 80 °C and compare this compound to water and octadecane, two other potential thermal energy storage materials. Furthermore, we examine the lithium nitrate-water phase diagram and accurately determine the enthalpies of fusion and melting points for lithium nitrate trihydrate ($\Delta H_{fus} = 287 \pm 7$ J·g^{-1}, $T_m = 30.1$ °C) and the lithium nitrate trihydrate-lithium nitrate eutectic point ($\Delta H_{fus} = 264 \pm 2$ J·g^{-1}, $T_m = 28.3$ °C).

15. SUBJECT TERMS
salt hydrate, thermal energy storage, phase change material, thermal transport, enthalpy of fusion

16. SECURITY CLASSIFICATION OF:			17. LIMITATION OF ABSTRACT:	NUMBER OF PAGES	19a. NAME OF RESPONSIBLE PERSON (Monitor)
a. REPORT	b. ABSTRACT	c. THIS PAGE			Karla Strong
Unclassified	Unclassified	Unclassified	SAR	24	19b. TELEPHONE NUMBER *(Include Area Code)* N/A

Thermophysical Properties of Lithium Nitrate Trihydrate from -20 °C to 80 °C

Patrick J. Shamberger[1]*, *Timothy Reid*[1,2]

[1] Thermal Sciences & Materials Branch, Materials and Manufacturing Directorate, Air Force Research Laboratory, Wright-Patterson AFB, OH 45433

[2] University of Dayton Research Institute, University of Dayton, Dayton, OH 45469

RECEIVED DATE: (To be entered by editors)

* Phone: +1 (937) 255-6809. Fax: +1 (937) 255-2176. E-mail: patrick.shamberger@wpafb.af.mil

ABSTRACT: Lithium nitrate trihydrate is of interest as a thermal energy storage material, due to its large specific and volumetric heats of fusion and its low melting temperature. Here, we report the thermophysical properties of solid and liquid lithium nitrate trihydrate at temperatures between -20 °C and 80 °C and compare this compound to water and octadecane, two other potential thermal energy storage materials. Furthermore, we examine the lithium nitrate-water phase diagram and accurately determine the enthalpies of fusion and melting points for lithium nitrate trihydrate (ΔH_{fus} = 287 ± 7 J·g^{-1}, T_m = 30.1 °C) and the lithium nitrate trihydrate-lithium nitrate eutectic point (ΔH_{fus} = 264 ± 2 J·g^{-1}, T_m = 28.3 °C).

KEYWORDS: salt hydrate, thermal energy storage, phase change material, thermal transport, enthalpy of fusion

Approved for public release; distribution unlimited.

INTRODUCTION

Thermal management of aerospace systems and components is a critical element of meeting both current and future technological goals for the United States Air Force (USAF). [1] This challenge is made more demanding by trends in component miniaturization, increasing power output of components, decreases in traditional aircraft heat sinks, and the prevalence of thermal transients on USAF platforms. For thermal management purposes, thermal energy storage (TES) materials are of great utility, as they absorb transient pulses of heat, averaging heat loads over greater time scales, thereby decreasing the mass and volume of remaining thermal management elements.

In practice, materials which undergo a solid-liquid phase transition (commonly referred to as 'phase-change materials') are observed to reversibly absorb and release large quantities of heat over very small temperature ranges. [2] Of this class of materials, the paraffins have been widely adopted as engineering materials, due to the wide range of melting temperatures observed in different paraffins (-180 to 80 °C), their predictable melting and crystallization behaviors, and the workability and non-toxicity of the basic materials. In comparison, a number of salt hydrates have attracted interest which have volumetric storage densities nearly double those of paraffins (due principally to the higher density of the salt hydrates). [2-4] However, very few of the thermophysical parameters of these salt hydrate systems are known within a reasonable degree of certainty. This limits comparison with other known TES materials, as well as high-fidelity computational simulations of TES components based on salt hydrates.

This paper describes the thermophysical properties of one candidate salt hydrate system, lithium nitrate trihydrate ($LiNO_3$-$3H_2O$), recently investigated at the USAF Research Laboratory. $LiNO_3$-$3H_2O$ melts at ~30 °C, and offers double the volumetric energy densities (~400 $MJ \cdot m^{-3}$) of comparable melting-point paraffins. [2-4] Here, we report the heat capacity, thermal conductivity and diffusivity, density, viscosity, and vapor pressure of $LiNO_3$-$3H_2O$ between -20 °C and 80 °C, as determined by a number of analytical techniques. The thermophysical properties of this compound are compared against the properties of water and octadecane

Approved for public release; distribution unlimited.

($C_{18}H_{38}$), a paraffin with a similar melting point. Furthermore, we investigate the melting point and heat of fusion of $LiNO_3$-$3H_2O$ and the $LiNO_3$-$3H_2O$/$LiNO_3$ eutectic point.

EXPERIMENTAL METHODS

Lithium nitrate trihydrate ($LiNO_3$-$3H_2O$) samples were synthesized by adding stoichiometric quantities of de-ionized water to as-received anhydrous lithium nitrate (>99%, Alfa Aesar). A second batch of $LiNO_3$-$3H_2O$ was synthesized from de-ionized water and as-received high purity anhydrous lithium nitrate (>99.98%, metals basis, Alfa Aesar) in order to characterize the effect of purity on undercooling. Anhydrous lithium nitrate was weighed in a sealed vial to minimize water absorption, after which a calculated amount of water was added. Weight fractions of samples were determined by mass using a digital balance and the estimated uncertainty is $u(x) = 0.2$ wt%.

A TA instruments Q2000 Differential Scanning Calorimeter (DSC) was used to determine melting points and heats of fusion, as well as heat capacities. Heats of fusion were measured from melting peaks during heating at 2 °C·min^{-1}, after calibrating the DSC cell with a pure Indium standard (99.9%, supplied by TA instruments) to a reference value of $\Delta H_{fus} = 28.66$ J·g^{-1}. [5] Reported melting temperatures are the intercept of the baseline with the tangent of the DSC trace with the maximum slope. The uncertainty of temperature measurements was verified by the melting point of Indium (156.60 °C)[5] and is $u(T) = 0.2$ °C. The relative uncertainty of individual heat of fusion measurements is $u_r(\Delta H_{fus}) = 0.05$, based on repeated analysis of indium and pure water standards. Reported melting temperatures and enthalpies of fusion are averages of 6 different samples. Heat capacities were determined using the modulated DSC technique, after calibrating the cell with a sapphire standard. Relative uncertainty of heat capacity measurements is $u_r(C_p) = 0.05$, based on repeated analysis of sapphire and water reference standards. [6] Reported DSC heat capacities are averages of 3 different samples. All DSC samples were hermetically sealed in aluminum test pans during testing.

Thermal properties of the liquid (diffusivity, conductivity, and heat capacity) were analyzed by the transient

Approved for public release; distribution unlimited.

hot wire technique (PSL Systemtechnik Lambda 01/L) following ASTM D2717. [7] Prior to analysis, the instrument was calibrated with water at 15 °C and the temperature scale was calibrated using a high precision digital thermometer (GMH 3710), with manufacturer specified uncertainty of $u(T) = 0.01$ °C. Uncertainties of thermal diffusivity, thermal conductivity, and heat capacity are all estimated to be $u_r(\alpha, k, C_p) = 0.05$ based on repeated analysis of ultrapure water (18.2 MΩ·cm, ASTM/CAP/NCCLS Type I) and toluene standards. [8] Liquid $LiNO_3$-$3H_2O$ was poured into the hot wire sampling cup under an argon atmosphere. Porous cork stoppers were placed in the sample assembly's vent ports, allowing for gas expansion while minimizing the introduction of moisture. Reported thermal properties are averages of 10 measurements at each temperature.

Thermal transport properties of the solid (diffusivity, conductivity) were analyzed by the transient plane source technique (ThermTest Hot Disk TPS 2500S thermal constants analyzer). Heat capacities of the solid measured by DSC were utilized in the calculation of diffusivity and conductivity. Relative uncertainty of thermal conductivity and diffusivity measured by this system are estimated to be $u_r(\alpha, k, C_p) = 0.10$, based on repeated analysis of Vespel and Pyrex standards. Liquid $LiNO_3$-$3H_2O$ was loaded into a 12 mm diameter Teflon liquid cell with a 2 mm diameter sensor suspended in the center. The cell was sealed with a paraffin film to minimize the introduction of moisture, and was allowed to cool and solidify. Reported values are averages of 5 measurements at each temperature.

Liquid density was measured using an oscillating u-tube with viscosity correction and a reference oscillator (Rudolph Research Analytical DDM 2911 densitometer). The DDM 2911 was calibrated using pure water. Relative uncertainty of individual liquid density measurements is estimated to be $u_r(\rho) = 0.005$, based on repeated analysis of air and of a pure water standard. Liquid $LiNO_3$-$3H_2O$ was drawn into a syringe and capped under an argon atmosphere. The densitometer's u-tube was purged with N_2 and the outlet was fitted with a drying tube. The sample was introduced into the u-tube via the syringe. A fresh sample was used at each 10 °C temperature step from 30-90 °C. Solid densities were calculated from the crystal structure data for $LiNO_3$-$3H_2O$ as determined by x-ray and neutron diffraction. [9-10] Relative uncertainty of solid densities are

Approved for public release; distribution unlimited.

$u_r(\rho) = 0.002$, based on the reported uncertainty of the lattice parameters.

Kinematic viscosity was measured by flow rate through a glass capillary tube following ASTM D445. [11] The capillary tube calibration was verified using Cannon viscosity standard S2000 at 100 °C and was within 0.07% of the specified standard value (within the tolerance band of ±0.30% defined by ASTM D445). The relative uncertainty of viscosity measurements using this technique is estimated to be $u_r(\nu) = 0.01$, based on a comparison of inter-laboratory results of fluids with kinematic viscosities < 10 mm^2s^{-1}. [11] Liquid $LiNO_3$-$3H_2O$ was drawn into a glass capillary under an argon atmosphere, and the viscosity tube was fitted with molecular sieve drying tubes to minimize the exposure of the sample to atmospheric moisture. Reported viscosities are averages of 3 measurements.

Vapor pressure was measured directly by evacuating a glass vial containing a few grams of $LiNO_3$-$3H_2O$ to below 0.1 kPa. The vial was immersed completely in a water bath, and was allowed to thermally equilibrate. Pressure was measured using a digital diaphragm pressure gauge (Vacuubrand GMBH VSK 3000) with an uncertainty of $u(p)$ =0.02 kPa. Relative uncertainty of vapor pressure measurements using this method was $u_r(p) = 0.15$, based on analysis of a pure water reference material. Accuracy was likely limited due to thermal gradients existing within the pressure gauge.

RESULTS & DISCUSSION

Melting temperatures were measured by DSC for compositions along the $LiNO_3$-H_2O binary between 49.7 and 64.6 wt.% $LiNO_3$. This compositional range includes stoichiometric $LiNO_3$-$3H_2O$ (56.1 wt.% $LiNO_3$) and the $LiNO_3$-$3H_2O$/$LiNO_3$ eutectic composition (~61 wt.% $LiNO_3$). [12] Example melting curves are illustrated in Fig. 1. Stoichiometric $LiNO_3$-$3H_2O$ (56.1 wt.% $LiNO_3$) indicates a sharp melting peak with an onset melting temperature (T_m) at 30.1 °C. Compositions enriched in $LiNO_3$ display a superposition of two melting peaks, with the lower temperature T_m at 28.3 °C (corresponding to the $LiNO_3$-$3H_2O$/$LiNO_3$ eutectic temperature), and the higher temperature T_m at ~30 °C. As the concentration of $LiNO_3$ approaches the

Approved for public release; distribution unlimited.

$LiNO_3$-$3H_2O$/$LiNO_3$ eutectic composition, the higher temperature peak disappears (Fig. 1). At lower concentrations of $LiNO_3$, a significant fraction of melting still occurs at or just below ~30 °C, but melting no longer starts at a well-defined temperature. Additionally, a second melting peak is observed at ~-23 °C, corresponding to the H_2O/$LiNO_3$-$3H_2O$ eutectic temperature. This melting peak is not observed in all cases, as subcooling prevents crystallization in some runs. Melting temperatures (both T_m, the onset of the melting peak and T_{pk}, the temperature of the maximum of the melting peak) are illustrated on Fig. 2, alongside data originally reported by Campbell and Bailey (1958). [12] In all cases, the observations reported here are consistent with those previously reported results.

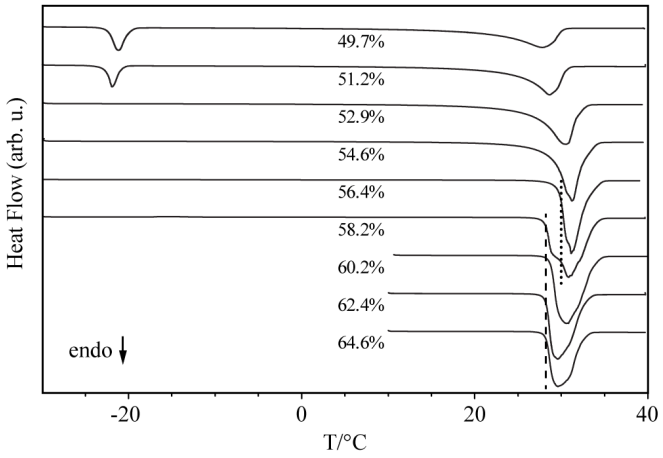

Figure 1. Representative DSC profiles of $LiNO_3$-H_2O solutions. Composition in wt% $LiNO_3$ is indicated on the figure. Dashed line indicates the eutectic point T_m (28.3 °C), dotted line indicates the T_m of $LiNO_3$-$3H_2O$ (30.1 °C).

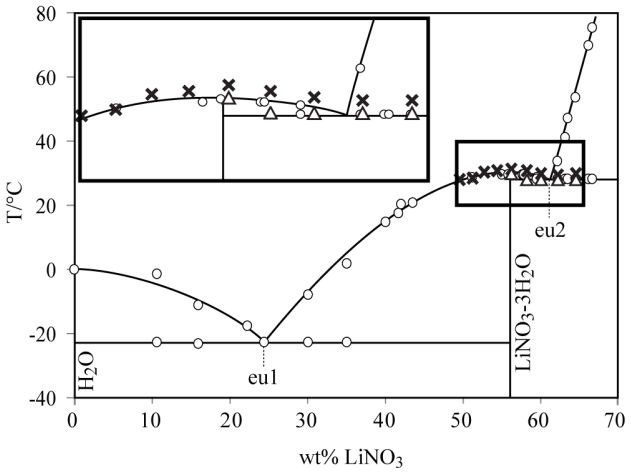

Approved for public release; distribution unlimited.

Figure 2. Phase diagram of $LiNO_3$-$3H_2O$ system. White circles from Campbell & Bailey (1958). [12] Onset of melting T_m (triangles) and maximum of the melting peak T_{pk} (x's) are indicated for the compositions in this study. Eutectic points eu1 and eu2 are illustrated on the phase diagram.

The enthalpy of fusion (ΔH_{fus}) and entropy of fusion (ΔS_{fus}) of $LiNO_3$-$3H_2O$ (56.1 wt.% $LiNO_3$) and of the approximate composition of the $LiNO_3$-$3H_2O$/$LiNO_3$ eutectic (61.6 wt.% $LiNO_3$) were both determined by DSC (Table 1). The latter composition involves melting of two distinct phases: $LiNO_3$-$3H_2O$ and $LiNO_3$. [12] Reported melting temperatures and enthalpies of fusion are averages of 6 independent samples; uncertainties are $\pm 2\sigma_{\bar{x}}$ (where $\sigma_{\bar{x}}$ is the standard deviation of the mean) and define an interval with a confidence level of 95%. These latent heats are 18% and 8% larger than the specific heat of fusion of octadecane (244 $J \cdot g^{-1}$), but 13% and 20% lower than the specific heat of fusion of pure water (334 $J \cdot g^{-1}$). [13] Enthalpy of fusion of $LiNO_3$/H_2O mixtures decrease nearly linearly away from stoichiometric $LiNO_3$-$3H_2O$ composition.

Table 1. T_m, ΔH_{fus}, and ΔS_{fus} of $LiNO_3$-$3H_2O$ and the $LiNO_3$-$3H_2O$/$LiNO_3$ eutectic

	wt% $LiNO_3$ [a]	T_m [a]	ΔH_{fus} [b]		ΔS_{fus} [b]	
		(°C)	($J \cdot g^{-1}$)	($J \cdot mole^{-1}$)	($mJ \cdot K^{-1} \cdot g^{-1}$)	($mJ \cdot K^{-1} \cdot mole^{-1}$)
$LiNO_3$-$3H_2O$	56.1%	30.1	287 ±7	2.33 ±0.06	946 ±23	7.69 ±0.19
$LiNO_3$-$2.39H_2O$	61.6%	28.3	264 ±2	2.36 ±0.02	876 ±7	7.82 ±0.06

[a] $u(x) = 0.2$ wt%, $u(T) = 0.2$ °C

[b] reported uncertainty is $\pm 2\sigma_{\bar{x}}$ of 6 different samples

Density of liquid $LiNO_3$-$3H_2O$ was measured with a commercial densitometer at temperatures between 35 °C and 80 °C. Solid densities are calculated from X-ray and neutron diffraction data collected at -153 °C and 22 °C (Table 2, Fig. 3). [9, 10] Experimental data are all well described by a simple linear dependence on T over this temperature range.

$$\rho = A + BT \qquad \text{(eq. 1)}$$

Here, ρ is the density (in $g \cdot cm^{-3}$), T is the temperature (in °C), and A and B are parameters fit to the data.

Approved for public release; distribution unlimited.

For the solid, A = 1.5794 and B =-0.0002; for the liquid, A = 1.4666 and B = -0.0012. Deviation of experimental data from the linear fit is <0.1 %. The density of $LiNO_3$-$3H_2O$ is ~40% (liquid) to ~80% (solid) greater than that of water, and is ~80% (liquid and solid) greater than that of paraffins. Volumetric thermal expansion (α_V) of $LiNO_3$-$3H_2O$ is calculated numerically from the density data, and is also illustrated in Fig. 3. The average α_V of solid $LiNO_3$-$3H_2O$ is 0.013 %·°C^{-1} between -153 °C and 22 °C. In liquid $LiNO_3$-$3H_2O$, α_V increases from 0.08 %·°C^{-1} at 35 °C to 0.09 %·°C^{-1}at 80 °C. Thermal expansion of liquid $LiNO_3$-$3H_2O$ is comparable to that of pure water over the same temperature range (0.035 %·°C^{-1} at 35 °C to 0.065 %·°C^{-1} at 80 °C). Volumetric expansion and contraction during melting/crystallizing were calculated by linearly extrapolating temperature-density trends to the transition temperature. During crystallization, $LiNO_3$-$3H_2O$ contracts by 10.0%. Thus, $LiNO_3$-$3H_2O$ differs from pure water which expands during freezing, and is comparable to the volumetric expansion of octadecane upon melting (9.8%).

Table 2. Density ρ of $LiNO_3$-$3H_2O$

T (°C)	ρ [a] (g·cm^{-3})	Technique	Phase	Ref.
-153.15	1.610	Diffraction	solid	(10)
21.85	1.575	Diffraction	solid	(10)
35	1.425	Densitometer	liquid	
40	1.420	Densitometer	liquid	
45	1.413	Densitometer	liquid	
50	1.408	Densitometer	liquid	
55	1.402	Densitometer	liquid	
60	1.395	Densitometer	liquid	
65	1.390	Densitometer	liquid	
70	1.384	Densitometer	liquid	
75	1.378	Densitometer	liquid	
80	1.372	Densitometer	liquid	

Approved for public release; distribution unlimited.

[a] $u_r(\rho)_{sol} = 0.002$; $u_r(\rho)_{liq} = 0.005$

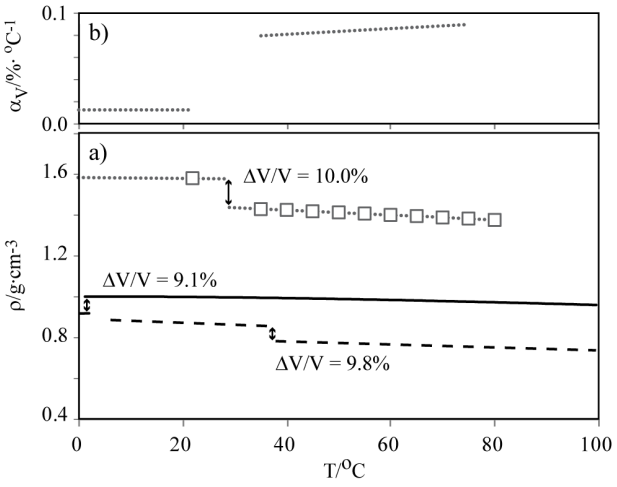

Figure 3. a) Density ρ and b) Volumetric thermal expansion α_V of $LiNO_3$-$3H_2O$ as measured by densitometer and as calculated from diffraction data (squares). [9, 10] Grey dotted line is the linear fit to the data. Density of H_2O (black solid line) and $C_{18}H_{38}$ (black dashed line) are included for reference. [3, 8] Volume contraction or expansion $\Delta V/V$ upon melting is calculated by extrapolating densities to T_m.

The volumetric heat of fusion of $LiNO_3$-$3H_2O$, calculated from calorimetric and density data, is 452 MJ·m^{-3} for the solid phase (just below T_m) and 409 MJ·m^{-3} for the liquid phase (just above T_m). Assuming that the eutectic has approximately the same density as stoichiometric $LiNO_3$-$3H_2O$, the volumetric heat of fusion of the $LiNO_3$-$3H_2O$/$LiNO_3$ eutectic is ~415 MJ·m^{-3} for the solid phase (just below T_m) and ~375 MJ·m^{-3} for the liquid phase (just above T_m). These values are ~120% (stoichiometric $LiNO_3$-$3H_2O$) or ~100% (eutectic $LiNO_3$-$3H_2O$/$LiNO_3$) larger than the volumetric heats of fusion of octadecane (Fig. 4). [3] Similarly, these values are ~35% or ~25% larger than the volumetric heats of fusion of water. [8, 13] Thus, both compositions of interest represent some of the largest known values for volumetric heat of fusion in the low temperature range (0 °C to 100 °C). This higher density of $LiNO_3$-$3H_2O$ relative to that of water or paraffins is largely responsible for the high volumetric latent heat of fusion of $LiNO_3$-$3H_2O$ relative to those materials.

Approved for public release; distribution unlimited.

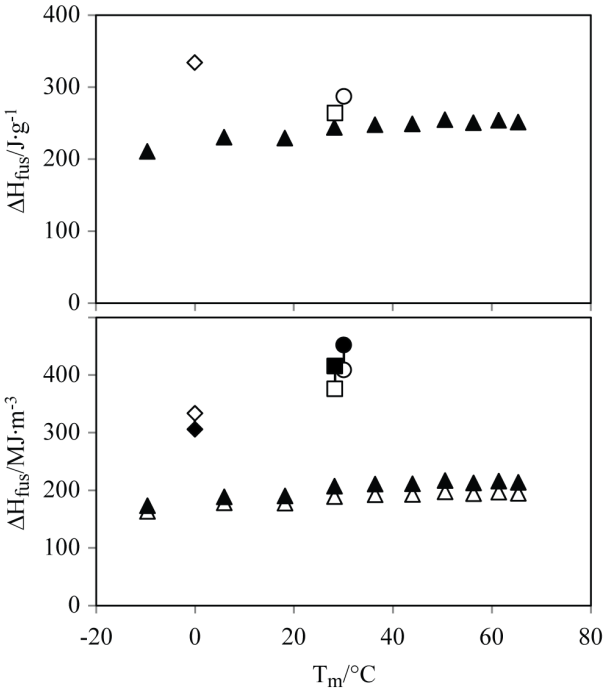

Figure 4. a) Specific heat of fusion ΔH_{fus}, and b) volumetric ΔH_{fus} for $LiNO_3$-$3H_2O$ (circles), the $LiNO_3$-$3H_2O$/$LiNO_3$ eutectic (squares), H_2O (diamonds), and simple paraffins with even numbers of carbon atoms (triangles). [3, 8, 13] Volumetric ΔH_{fus} calculated for solid densities (filled symbols) and liquid densities (empty symbols) are connected by a line.

Constant pressure heat capacity C_p of $LiNO_3$-$3H_2O$ is measured by DSC (Table 3) and by the transient hot wire technique (Table 4), and is illustrated as a function of temperature in Fig. 5. Heat capacity of liquid $LiNO_3$-$3H_2O$ at temperatures just above the phase transition is 2.8 $J \cdot g^{-1} \cdot K^{-1}$, while heat capacity of solid $LiNO_3$-$3H_2O$ at temperatures just below the phase transition is 1.8 $J \cdot g^{-1} \cdot K^{-1}$. Liquid heat capacity is measured by both DSC and hot wire techniques; both measurements are within experimental uncertainty of each other. Liquid heat capacity is nearly constant across the temperature investigated (35 °C to 85 °C), and is ~15%-25% larger than the heat capacity of octadecane and 35% smaller than the heat capacity of water over the same temperature range. Solid heat capacity increases linearly from -25 °C to 15 °C (at 0.0041 $J \cdot g^{-1} \cdot K^{-2}$, at approximately the same slope as water), but is less than both water and octadecane over this temperature range.

Approved for public release; distribution unlimited.

Table 3. Heat Capacity C_p of $LiNO_3$-3H_2O at selected temperatures, as measured by DSC

T [a] (°C)	C_p [a] ($J \cdot g^{-1} \cdot K^{-1}$)	Phase
-20	1.59	solid
-10	1.63	solid
0	1.67	solid
10	1.71	solid
15	1.73	solid
40	2.76	liquid
50	2.77	liquid
60	2.76	liquid
70	2.77	liquid
80	2.76	liquid

[a] $u(T) = 0.2$ °C, $u_r(C_p) = 0.05$

Table 4. Thermal properties of $LiNO_3$-3H_2O, as measured by the transient hot wire technique

T [a] (°C)	k [a] ($W \cdot m^{-1} \cdot K^{-1}$)	α [a] ($m^2 \cdot s^{-1}$)	C_p [a] ($J \cdot g^{-1} \cdot K^{-1}$)	Phase
35	0.584	14.1	2.91	liquid
40	0.581	14.0	2.91	liquid
45	0.587	14.1	2.94	liquid
50	0.583	14.1	2.94	liquid
55	0.585	14.1	2.96	liquid
60	0.588	14.2	2.98	liquid
65	0.588	14.2	2.99	liquid
70	0.588	14.2	3.00	liquid
75	0.595	14.3	3.03	liquid

Approved for public release; distribution unlimited.

80	0.611	14.5	3.07	liquid

[a] $u_r(T) = 0.2$ °C, $u_r(k, \alpha, C_p) = 0.05$

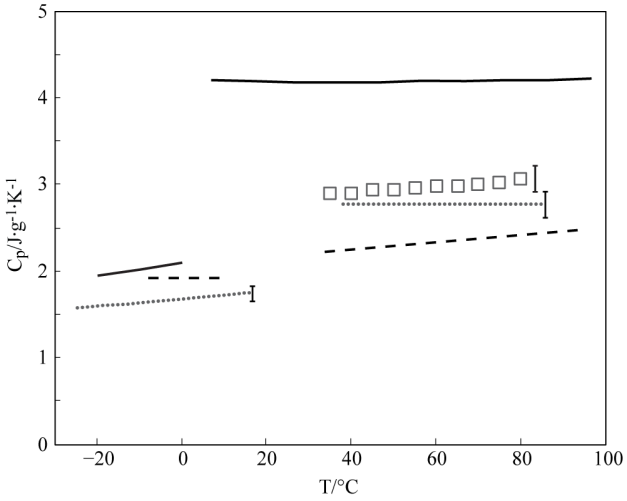

Figure 5. Constant pressure heat capacity C_p of $LiNO_3$-$3H_2O$, as measured by the hot wire technique (squares) and by DSC (dotted line). Values for H_2O (solid line) and $C_{18}H_{38}$ (dashed line) are included for reference. [3, 6]

Thermal conductivity (Fig. 6) and thermal diffusivity (Fig. 7) of solid and liquid $LiNO_3$-$3H_2O$ were measured between -20 °C and 80 °C using the transient hot wire (liquid, Table 4) and transient plane source (solid, Table 5) methods. Liquid thermal conductivity (0.59 $W \cdot m^{-1} \cdot K^{-1}$) and thermal diffusivity ($14.1 \cdot 10^{-8}$ $m^2 \cdot s^{-1}$) remain constant within experimental uncertainty between 35 °C and 80 °C, and are both very near the values for pure water (0.62-0.67 $W \cdot m^{-1} \cdot K^{-1}$, 14.9-15.7$\cdot 10^{-8}$ $m^2 \cdot s^{-1}$). Solid thermal conductivity (0.75 $W \cdot m^{-1} \cdot K^{-1}$) and thermal diffusivity ($29 \cdot 10^{-8}$ $m^2 \cdot s^{-1}$) also remain constant within experimental uncertainty between -20 °C and 20 °C, but are only ~25%-35% of the values for pure water. Liquid thermal conductivity and thermal diffusivity are ~400% and ~200% higher than that of octadecane, while solid thermal conductivity and thermal diffusivity are ~200% and ~120% higher. Given an identical temperature gradient, the local heat flux density is proportional to the thermal conductivity. Thus, TES components based on $LiNO_3$-$3H_2O$ may be expected to have higher cooling power densities than those based on paraffins.

Approved for public release; distribution unlimited.

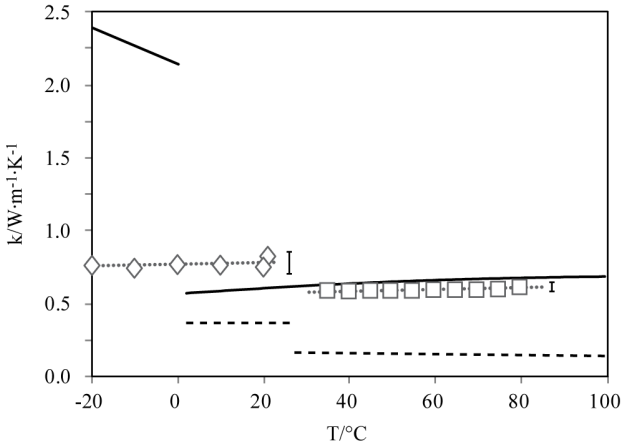

Figure 6. Thermal conductivity k of $LiNO_3$-$3H_2O$ as measured by the hot wire technique (squares) and the hot disk technique (diamonds). Values for H_2O (black solid line) and $C_{18}H_{38}$ (black dashed line) are included for reference. [3, 8]

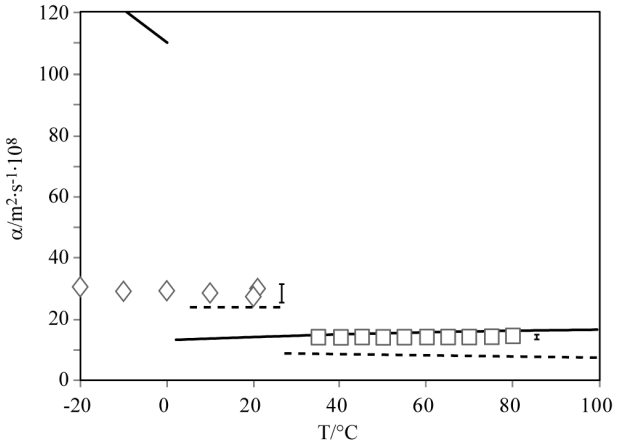

Figure 7. Thermal diffusivity α of $LiNO_3$-$3H_2O$ as measured by the hot wire technique (squares) and the hot disk technique (diamonds). Values for H_2O (solid line) and $C_{18}H_{38}$ (dashed line) are included for reference. [3, 8]

Table 5. Thermal transport properties of solid $LiNO_3$-$3H_2O$, as measured by the transient plane source technique

T (°C)	k [a] ($W \cdot m^{-1} \cdot K^{-1}$)	α [a] ($m^2 \cdot s^{-1}$)	Phase
21	0.82	$30 \cdot 10^{-8}$	solid
20	0.75	$27 \cdot 10^{-8}$	solid

Approved for public release; distribution unlimited.

10	0.76	$28 \cdot 10^{-8}$	solid
0	0.77	$29 \cdot 10^{-8}$	solid
-10	0.74	$29 \cdot 10^{-8}$	solid
-20	0.76	$30 \cdot 10^{-8}$	solid

[a] $u_r(k, \alpha) = 0.10$

Kinematic viscosity of liquid $LiNO_3$-$3H_2O$ was measured with a commercial viscometer at temperatures between 35 °C and 80 °C (Table 6). Absolute (dynamic) viscosity was calculated from kinematic viscosity and from density measurements taken at the same temperatures (Fig. 8). Experimental data were fit with a polynomial equation as a function of temperature, following a form previously used for hydrous $LiNO_3$ solutions). [14]

$$\eta = A + B/T + C/T^2 \qquad \text{(eq. 2)}$$

Here, η is absolute viscosity (in Pa·s), T is the temperature (in °C), and $A = 6.469 \cdot 10^{-4}$, B = 0.2778, and C = -2.386 are parameters fit to the data. Deviation of experimental data from the polynomial fit is <0.5%. Absolute viscosity of $LiNO_3$-$3H_2O$ is ~50% greater than that of octadecane, although the kinematic viscosity of $LiNO_3$-$3H_2O$ is ~15% less, due to the density difference between the two materials.

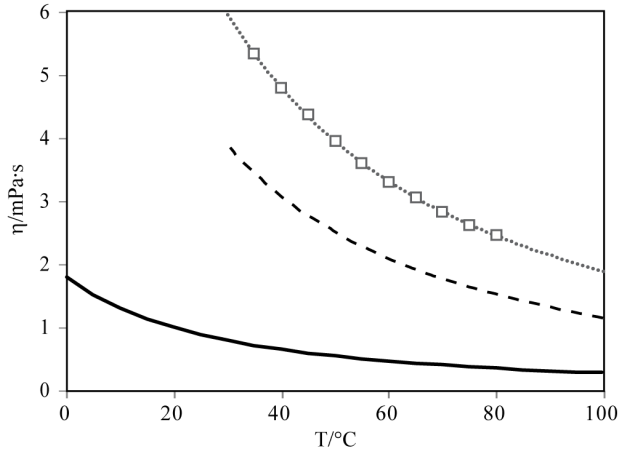

Figure 8. Absolute viscosity η of $LiNO_3$-$3H_2O$ (squares). Grey dotted line is the polynomial fit to the data. Values for H_2O (solid line) and $C_{18}H_{38}$ (dashed line) are included for reference. [3, 8]

Approved for public release; distribution unlimited.

Table 6. Kinematic ν and Absolute viscosity η of $LiNO_3$-3H_2O

T (°C)	ν [a] ($m^2 \cdot s^{-1}$)	η [a] (mPa·s)	Phase
35	$3.75 \cdot 10^{-6}$	5.34	liquid
40	$3.38 \cdot 10^{-6}$	4.80	liquid
45	$3.09 \cdot 10^{-6}$	4.37	liquid
50	$2.81 \cdot 10^{-6}$	3.96	liquid
55	$2.57 \cdot 10^{-6}$	3.60	liquid
60	$2.37 \cdot 10^{-6}$	3.31	liquid
65	$2.20 \cdot 10^{-6}$	3.06	liquid
70	$2.05 \cdot 10^{-6}$	2.84	liquid
75	$1.91 \cdot 10^{-6}$	2.63	liquid
80	$1.79 \cdot 10^{-6}$	2.46	liquid

[a] $u_r(\nu,\mu) = 0.01$

Vapor pressure data are fit with the August equation, assuming a temperature-independent heat of vaporization (Fig. 9).

$$log_{10}P = A - B/T \qquad \text{(eq. 3)}$$

Here, p is the pressure (in kPa), T is the temperature (in K), and A = 8.990 and B = 2711 are parameters fit to the data. This model is adequate to describe the vapor pressure-temperature relationship, given the relatively large uncertainty of the data reported here. The equilibrium vapor pressure of $LiNO_3$-3H_2O is only ~25% that of liquid water, representing a significant negative deviation from Raoult's Law (which would predict a vapor pressure of $LiNO_3$-3H_2O ~60% that of liquid water, assuming Li^+ and NO_3^- are nonvolatile solutes).

Approved for public release; distribution unlimited.

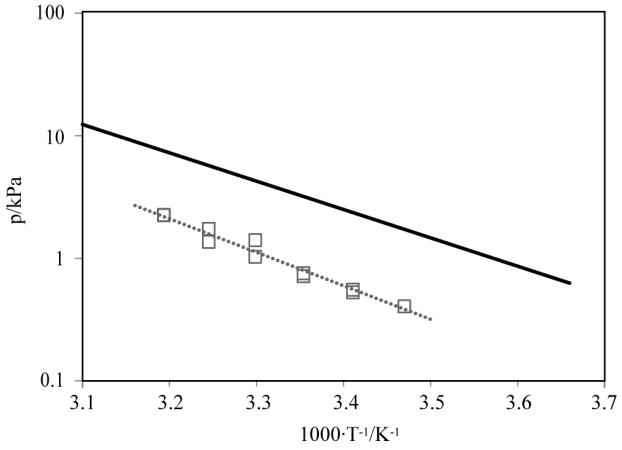

Figure 9. Equilibrium vapor pressure p of $LiNO_3$-$3H_2O$. Grey dotted line is the fit with the August equation, as described in the text. Values for H_2O (solid line) are included for reference. [3, 8]

The equilibrium vapor pressure of $LiNO_3$-$3H_2O$ is ~25% relative humidity, which is much lower than typical ambient relative humidity in laboratory environments (~40%-60%). Thus, the low equilibrium vapor pressure of $LiNO_3$-$3H_2O$ is responsible for its hygroscopic behavior. In fact, crystalline $LiNO_3$-$3H_2O$ left exposed to ambient air was observed to absorb moisture and to deliquesce, as the melting point of the material decreases with an increase in water content (Fig. 2).

Certain salt hydrates are known to exhibit a large temperature difference (ΔT) between the equilibrium crystallization temperature, and the temperature at which crystallization actually takes place. This undercooling is related to the large energy barrier required for homogenous nucleation, and can cause potential problems for TES components by limiting their ability to regenerate without active cooling. [2, 15, 16] In $LiNO_3$-$3H_2O$, ΔT is relatively large (>10 °C), and is even larger with higher purity starting material (Table 7). This observation is consistent with the hypothesis that impurities in the starting material serve as potential nucleation sites for crystalline $LiNO_3$-$3H_2O$, proposed based on observations of undercooling in a variety of materials systems. [16] However, it is unclear whetehr those impurities will remain stable over large periods of time or at higher temperatures. Research into stable nucleation agents to promote heterogeneous nucleation is ongoing in the authors' research group. [17]

Approved for public release; distribution unlimited.

Table 7. Undercooling ΔT of $LiNO_3$-$3H_2O$ as a function of starting material

	ΔT [a]		N [b]
	avg. (°C)	2σ (°C)	
Lithium Nitrate, anhyd. 99.98%	39.3	14.3	19
Lithium Nitrate, anhyd. 99%	14.9	2.3	5

[a] $u(T) = 0.2$ °C

[b] reported values are averages of N independent measurements

CONCLUSIONS

The thermophysical properties of $LiNO_3$-$3H_2O$ are measured at temperatures between -20 °C and 80 °C. These are compared against the properties of water and octadecane, two other potential thermal energy storage materials. Both $LiNO_3$-$3H_2O$ (287 $J \cdot g^{-1}$, 409 $MJ \cdot m^{-3}$) and the $LiNO_3$-$3H_2O$/$LiNO_3$ eutectic point (264 $J \cdot g^{-1}$, ~375 $MJ \cdot m^{-3}$) have very high volumetric energy storage density, which even exceeds that of water. Furthermore, these two compositions have a higher specific energy density, thermal conductivity and thermal diffusivity than that of comparable paraffins (octadecane). Thus, $LiNO_3$-based salt hydrates are very competitive a thermal energy storage materials, and excel in applications where volume is at a premium. Further studies of other salt hydrate systems are needed to evaluate their potential as TES materials and to establish compositional trends in material properties.

FUNDING SOURCES: The authors thank the Air Force Research Laboratory, Materials and Manufacturing Directorate for providing necessary financial support to carry out the present work.

REFERENCES:

Approved for public release; distribution unlimited.

(1) Office of the U.S. Air Force Chief Scientist (AF/ST). *Report on Technology Horizons: A Vision for Air Force Science & Technology During 2010-2030*; AF/ST-TR-10-01-PR, 2010. http://www.af.mil/information/technologyhorizons.asp (accessed Oct 24, 2011).

(2) Mehling, H.; Cabeza, L. F. *Heat and Cold Storage with PCM: an Up to Date Introduction into Basics and Applications*; Springer: Berlin, Germany, 2008.

(3) Humphries, W. R.; Griggs, E. I. *A Design Handbook for Phase Change Thermal Control and Energy Storage Devices*; NASA-TP-1074, NTIS: Springfield, VA, 1977.

(4) Hale, D. V.; Hoover, M. J.; and O'Neil, M. J. *Phase Change Materials Handbook*; NASA-CR-61363, Lockheed Missiles & Space Company: Huntsville, AL, 1971.

(5) Archer, D. G.; Rudtsch S. Enthalpy of Fusion of Indium: A Certified Reference Material for Differential Scanning Calorimetry. *J. Chem. Eng. Data* **2003,** *48*, 1157-1163.

(6) Chase, M. W., Jr. *NIST-JANAF Themochemical Tables*, 4th Ed.; J. Phys. Chem. Ref. Data Monograph 9; American Institute of Physics: Washington, DC, 1998.

(7) ASTM Standard D2717, 1995(2009) *Standard Test Method for Thermal Conductivity of Liquids*; ASTM International: West Conshohocken, PA, 2009, DOI: 10.1520/D2717-95R09. www.astm.org (accessed Oct 24, 2011).

(8) Lemmon, E.W.; McLinden, M.O.; Friend, D.G. Thermophysical Properties of Fluid Systems. In *NIST Chemistry WebBook*; Linstrom, P. J.,Mallard, W.G., Eds.; NIST Standard Reference Database Number 69; NIST: Gaithersburg, MD. http://webbook.nist.gov (accessed Oct 24, 2011).

(9) Hermansson, K.; Thomas, J. O.; Olovsson, I. Hydrogen Bond Studies. CXX. An X-ray Determination of the Crystal Structure of LiNO3-3H2O. *Acta Crystallogr.* **1977**, *B33*, 2857-2861.

Approved for public release; distribution unlimited.

(10) Hermansson, K.; Thomas, J. O.; Olovsson, I. Hydrogen Bond Studies. CXXXVIII. Neutron Diffraction Studies of LiNO3-3H2O at 120 and 295 K. *Acta Crystallogr.* **1980**, *B36*, 1032-1040.

(11) ASTM Standard D445, 2011a *Standard Test Method for Kinematic Viscosity of Transparent and Opaque Liquids (and Calculation of Dynamics Viscosity)*; ASTM International: West Conshohocken, PA, 2011, DOI: 10.1520/D0445-11A. www.astm.org (accessed Oct 24, 2011).

(12) Campbell, A. N.; Bailey, R. A. The System Lithium Nitrate-Ethanol-Water and Its Component Binary Systems. *Can. J. Chem.* **1958**, *36*, 518-536.

(13) Lide, D. R. *CRC Handbook of Chemistry and Physics*, 90th Ed.; CRC Press: Boca Raton, FL, 2010.

(14) Iyoki, S.; Iwasaki, S.; Kuriyama, Y.; Uemura, T. Densities, Viscosities, and Surface Tensions for the Two Ternary Systems H2O + LiBr + LiI and H2O + LiCl + LiNO3. *J. Chem. Eng. Data* **1993**, *38*, 302-305.

(15) Porter, D. A.; Easterling, K. E.; Sherif, M.Y. *Phase Transformations in Metals and Alloys*, 3rd ed.; CRC Press: Boca Raton, FL, 2009.

(16) Turnbull, D. The Undercooling of Liquids. *Sci. Am.* **1965**, *212*, 38-46.

(17) Shamberger, P. J.; Forero, D.E. Towards High Energy Density, High Conductivity Thermal Energy Storage Composites. In *Proc. of the ASME 2012 3rd Micro/Nanoscale Heat & Mass Transfer International Conference*, Atlanta, GA, Mar 3-6, 2012; ASME: New York, NY, 2012.

SYNOPSIS TOC.

Approved for public release; distribution unlimited.

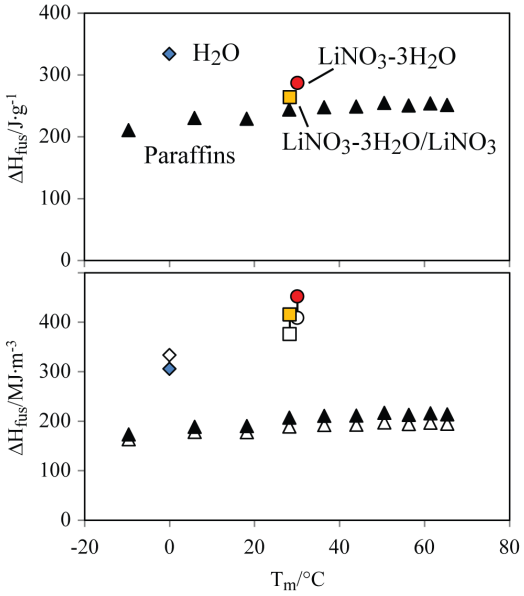

Approved for public release; distribution unlimited.